Materials Science & Engineering A 707 (2017) 12–15

Contents lists available at ScienceDirect

Materials Science & Engineering A

journal homepage: www.elsevier.com/locate/msea

Effect of crystallographic orientation on impression creep behaviors of single crystal based on crystal plasticity theory

Wuzhu Yan*, Xin Yuan, Wanjia Zhao, Zhufeng Yue

Department of Engineering Mechanics, School of Mechanics, Civil Engineering and Architecture, Northwestern Polytechnical University, Xi'an, Shaanxi, PR China

ARTICLE INFO

Keywords:
Crystal plasticity
Impression creep
Crystallographic orientation
Finite elements

ABSTRACT

The present work aims to reveal the effect of crystallographic orientation on impression creep responses of single crystal alloys. For this purpose, crystal plasticity finite element (FE) method was employed to simulate the process of impression creep performed on [001]-, [011]- and [111]- oriented nickel based single crystal alloys. The determination of crystallographic creep parameters by impression creep was explored and compared among differently oriented single crystals. The result shows that the stress distribution and surface morphology induced by impression creep exhibit anisotropic patterns which are strongly dependent on crystallographic orientation. The determination of creep stress exponent is independent on crystallographic orientation.

1. Introduction

Nickel based single crystal (SC) super alloys has been widely used in turbine blades of aircraft engine and gas turbine due to its excellent performance at elevated temperature. With the increase of inlet temperature of turbine blades, creep induced deformation greatly reduces the work efficiency of turbines blades. Meanwhile, creep has become the most important failure mode of turbine blades. Hence, a reliable evaluation of creep resistance of nickel based SC super alloys is essential for the maintenance of in-service turbine blades.

The anisotropic creep properties of nickel base SC super alloys were usually tested by conventional tensile creep or double shear creep. However, conventional creep tests are not operable for in-service turbine blades due to their strict requirements in specimen sizes and geometries. In order to overcome the shortages of conventional creep tests, the impression creep, an efficient technique in which a ball or a conical indenter was replaced by a flat ended cylindrical indenter owing to steady punching stress during creep, has brought about the widespread attention due to its simple, fast and non-destructive merits. The impression creep technique was first exploited by Yu and Li [1], they found that the penetration rate of the punch shows a power law dependence on punching stress, and the creep parameters can be well correlated with those from tensile creep test:

$$\dot{h} = C_i \sigma_N^{n_i} \tag{1}$$

$$n = n_i = \frac{\Delta \ln \dot{\varepsilon}}{\Delta \ln \sigma_{eff}} = \frac{\Delta \ln \dot{h}}{\Delta \ln \sigma_N} \tag{2}$$

where $\dot{h}$ is the penetration rate of the punch, σ_N is the punching stress, $\dot{\varepsilon}$ is the creep strain rate of tensile creep, σ_{eff} is the equivalent stress of tensile creep, C_i and n_i are the pre-factor and punching stress exponent of impression creep, n is the creep stress exponent of tensile creep. In the past decades, the impression creep technique has been validated by other independent studies [2–14].

In recent years, the impression creep technique was applied on SC materials. Yan [15] compared the impression creep and uniaxial tensile creep performed on nickel base SC super alloys, and explored the possibility of bridging these two kinds of creep tests. Xu [16] studied the crystallographic creep parameters and indentation creep surface morphology of nickel-based SC super alloys. However, the determination of crystallographic creep parameters of single crystals by impression creep has not been fully exploited due to the complex anisotropic response during impression creep. For single crystals, the penetration of the punch is realized by the crystallographic creep slipping driven by resolved shear stress, which is strongly affected by crystallographic orientation. So far, the crystallographic orientation sensitivity of impression creep performed on single crystals has not been fully investigated.

The present work aims to address the aforementioned gap by carrying our FE simulation of impression creep performed on nickel base SC super alloys. For this purpose, the crystallographic creep user materials subroutine was developed based on crystal plasticity theory. The effects of crystallographic orientation on penetration depth propagation, surface stress and surface deformation were revealed. Finally, the crystallographic creep parameters were determined by the linear regression approach for differently oriented single crystals.

* Corresponding author.
E-mail address: yanwuzhu@nwpu.edu.cn (W. Yan).

http://dx.doi.org/10.1016/j.msea.2017.08.118
Received 29 June 2017; Received in revised form 31 August 2017; Accepted 31 August 2017
Available online 01 September 2017
0921-5093/

2. Crystallographic creep constitution

The crystal plasticity model of creep was recently exploited in our recent work [17]. Only essential ingredients were outlined here for integrality.

The Norton's creep law is assumed for the second stage of creep, the resolved creep shear strain rate $\dot{\gamma}_c$ can be obtained by

$$\dot{\gamma}_c^{(\alpha)} = a(\tau^{(\alpha)})^n \tag{3}$$

where a and n are material parameters, and α specifies the slip system. When a load σ is applied, the resolved shear stress of slip system α can be calculated by

$$\tau^{(\alpha)} = \boldsymbol{\sigma} : \mathbf{P}^{(\alpha)} \tag{4}$$

with

$$\boldsymbol{P}^{(\alpha)} = \frac{1}{2}(\boldsymbol{m}^{(\alpha)}\boldsymbol{n}^{(\alpha)T} + \boldsymbol{n}^{(\alpha)}\boldsymbol{m}^{(\alpha)T}) \tag{5}$$

where $\boldsymbol{m}^{(\alpha)}$ represents the slip direction of slip system α and $\boldsymbol{n}^{(\alpha)}$ is the normal direction of the slip plane. The evolution of creep strain rate $\dot{\varepsilon}_c$ can be computed by

$$\dot{\varepsilon}_c = \sum_{\alpha=1}^{N} \dot{\gamma}_c^{(\alpha)} \boldsymbol{P}^{(\alpha)} \tag{6}$$

where N is the number of the active slip systems.

Assuming that the elastic behavior is not affected by the creep deformation, we have

$$\Delta\boldsymbol{\sigma}_e = \boldsymbol{D}^e : \Delta\boldsymbol{\varepsilon}_e \tag{7}$$

where $\boldsymbol{\varepsilon}_e$ and $\boldsymbol{\sigma}_e$ are the elastic strain tensor and elastic stress tensor, $\boldsymbol{D}^e$ is the fourth-order tensor of elastic constants:

$$\Delta\boldsymbol{\sigma}_e = \{\Delta\sigma_{11},\Delta\sigma_{22},\Delta\sigma_{33},\Delta\sigma_{12},\Delta\sigma_{13},\Delta\sigma_{23}\}^T \tag{8}$$

$$\Delta\boldsymbol{\varepsilon}_e = \{\Delta\varepsilon_{11},\Delta\varepsilon_{22},\Delta\varepsilon_{33},\Delta\varepsilon_{12},\Delta\varepsilon_{13},\Delta\varepsilon_{23}\}^T \tag{9}$$

$$\boldsymbol{D}^e = \begin{bmatrix} C_{11} & C_{12} & C_{12} & 0 & 0 & 0 \\ C_{12} & C_{11} & C_{12} & 0 & 0 & 0 \\ C_{12} & C_{12} & C_{11} & 0 & 0 & 0 \\ 0 & 0 & 0 & C_{44} & 0 & 0 \\ 0 & 0 & 0 & 0 & C_{44} & 0 \\ 0 & 0 & 0 & 0 & 0 & C_{44} \end{bmatrix} \tag{10}$$

where C_{11}, C_{12} and C_{44} can be written as a function of elastic modulus E, shear modulus G and Possion's ratio μ:

$$C_{11} = E,\ C_{12} = -\mu E,\ C_{44} = G \tag{11}$$

The relationship between the crystallographic coordinate system ([001]–[010]–[100]) and the global coordinate system (X–Y–Z) can be built by

$$\boldsymbol{D}' = \boldsymbol{T}\boldsymbol{D}^e\boldsymbol{T}^T \tag{12}$$

where $\boldsymbol{D}'$ and $\boldsymbol{T}$ are the deviatoric elastic stiffness tensor and the transformation tensor:

$$\mathbf{T} = \begin{bmatrix} l_1^2 & m_1^2 & n_1^2 & 2l_1m_1 & 2l_1n_1 & 2m_1n_1 \\ l_2^2 & m_2^2 & n_2^2 & 2l_2m_2 & 2l_2n_2 & 2m_2n_2 \\ l_3^2 & m_3^2 & n_3^2 & 2l_3m_3 & 2l_3n_3 & 2m_3n_3 \\ l_1l_2 & m_1m_2 & n_1n_2 & l_1m_2 + l_2m_1 & l_1n_2 + l_2n_1 & m_1n_2 + m_2n_1 \\ l_2l_3 & m_2m_3 & n_2n_3 & l_3m_2 + l_2m_3 & l_2n_3 + l_3n_2 & m_2n_3 + m_3n_2 \\ l_1l_3 & m_1m_3 & n_1n_3 & l_1m_3 + l_3m_1 & l_1n_3 + l_3n_1 & m_1n_3 + m_3n_1 \end{bmatrix} \tag{13}$$

where l, m and n are the cosine values of the angles between the crystallographic coordinate system ([0 0 1]–[0 1 0]–[1 0 0]) and the global coordinate system (x-y-z).

The above constitutive relationships were implemented into the FE code ABAQUS via a specially written user subroutine UMAT, and its effectiveness has been validated by independent studies of indentation behaviors of single crystal super alloys.

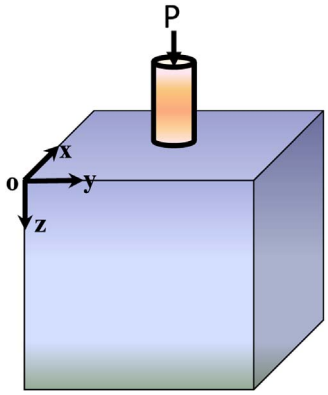

Fig. 1. Schematic view of the impression creep.

3. Model development

A schematic view of impression creep technique was shown in Fig. 1. A cubic solid was pressed by a rigid cylindrical punch. A constant load P was applied on the punch to generate a constant punching stress. The length of the cubic edge was 10 times the radius of the punch so as to avoid the boundary effect. The boundary conditions are pre-defined as following:

$$X = L,\ x = 0;\ Y = 0,\ y = 0;\ Z = -L,\ z = 0 \tag{14}$$

where L is the length of the cubic edge. The punch was only free in Z direction. The cubic specimen was meshed by C3D8R elements. The mesh was gradually refined as approaching to the indented zone. Contact properties between the punch and the specimen were defined as hard contact with no friction. Three representative crystallographic orientations were assigned to the impressed solid. For each case, the relationship between the global coordinate and the crystallographic coordinate was shown in Table 1. The mechanical properties input the finite element model were from nickel based single crystal super alloys at 900 °C as listed in Table 2.

4. Results and discussion

4.1. Effect of crystallographic orientation on impression creep curves

The penetration depth of the punch as a function of creep time was shown in Fig. 2. It can be seen that the largest and smallest penetration depths for the same creep time were associated with [111]- and [001]-orientations, respectively. This is because more slip planes were activated in [111] orientation, resulting in minimum slip resistance on the (111) crystallographic plane.

4.2. Effect of crystallographic orientation on resolved shear stress distribution

It is well known that the resolved shear stress is the main driven force for crystallographic slipping of SC super alloys. To some extent, the distribution of resolved shear stress on the impressed surface

Table 1
Relationship between the global coordinate and the crystallographic coordinate.

Global coordinate axis Crystallographic orientation	x	y	z
Case I	[1 0 0]	[0 1 0]	[0 0 1]
Case II	[1 0 0]	[0 1 $\bar{1}$]	[0 1 1]
Case III	[1 1 $\bar{2}$]	[$\bar{1}$ 1 0]	[1 1 1]